# Data analysis of spectral images for nonlinear optical biopsy

Anton de Boer
Studentnumber 3471446
Utrecht University

January 11, 2013

**Abstract**

This paper summarizes the research done for a bachelor thesis at the Molecular Biophysics department of Utrecht University. In the research, the tumorous skin of hairless mice will be scanned in vivo by a microendoscope to generate Two Photon Fluorescence- and Second Harmonic Generation spectral images. The images will then be analyzed to determine whether they can be used to discriminate between healthy and tumorous tissue. The setup is powered by a ultrashort pulse (140 fs) Titanium Sapphire Laser.

# Contents

# 1 Introduction

Before the establishment of the microscope by Antony van Leeuwenhoek in 1673[1], not much was known of the world on a micrometer scale. The smallest living creature known in that time was the cheese-mite[2] but after Van Leeuwenhoek discovered his 'kleyne diertgens'[1], the interest in the very small has been greatly increased resulting in many discoveries and new scientific disciplines. In the past century, many different microscopy techniques with all kinds of applications have been invented and improved. On of these for example, is the electron microscope, which can image individual atoms. In the molecular biophysics, many microscopy techniques are developed and used for the study of small organisms and organic matter like bacteria, cells, or DNA. Two of these techniques called Multi Photon Fluorescence Microscopy and Second Harmonic Generation, are of particular interest in this field of study because of their potential to optically determine the metabolism (chemical makeup) in organic cells. It is known that diseases like cancer affect the metabolism[3], meaning these imaging techniques could be used to indirectly identify these diseases in patients. In the future this could for instance, make it possible to replace surgical biopsies with an optical diagnosis by which tissue desecration is minimized. Multi Photon Fluorescence and Second Harmonic Generation imaging is real time, in high resolution and can be applied on living tissue (in vivo). Consequently, accurate diagnoses could be made easier and in a much shorter time period which can drastically increase the chances of survival of the patient, because treatment can commence in an earlier stage. In this research, a setup has been constructed to determine to what extend Multi Photon Fluorescence and Second Harmonic Generation Imaging can be used to detect tumor cells by scanning mice skin in vivo.

[1] old Dutch for 'little animals', van Leeuwenhoeks description of unicellular organism after he first discovered them.

# 2 Theoretical Background

Before the experiment can be discussed in greater detail, its theoretical background needs to be addressed. In this section, there will be a general discussion of the the two imaging techniques used in the experiment; Multi Photon Fluorescence and Second Harmonic Generation. It will then be explained how these techniques can be used to detect cancer in living tissue.

## 2.1 Multi Photon Fluorescence

Fluorescence is a naturally occurring physical phenomenon which was first described in 1852 by George Gabriel Stokes[4]. Stokes described the property of certain materials to convert ultraviolet light into light with a higher wavelength, making the emitted light visible to the human eye. This results in the fluorescent materials appearing to glow in the presence of an other (ultraviolet) light source. Many different substances have the potential to fluoresce, and this causes fluorescence to have a role in many applications. A common example would be the energy-saving lights where a current going through a tube lights up the gas inside, resulting in a practical and efficient light source. Another example is the high-visibility clothing road- and policemen sometimes wear. These clothes possess highly reflective elements as well as fluorescent materials, making the wearers better visible during the night. Fluorescence is also used in crime investigations: forensic researchers apply fluorescent compounds that attach to fingerprints, blood or other substances. This makes them visible in the presence of uv-light. From these examples, one can see fluorescence is a common phenomenon, which is present all around.

Similar to the forensic sciences, the experiment outlined in this paper relies on fluorescence as a contrast mechanism. In this section, fluorescence will be discussed in more detail: when the photons from a light source interact with a molecule or atom in a fluorescent

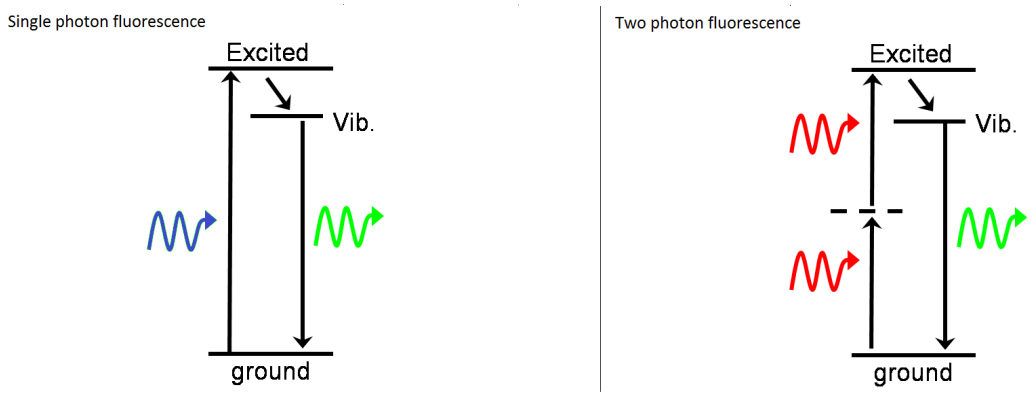


Figure 1: On the left; an electron residing in the ground states absorbs a photon and gets excited. On the right, two photons are simultaneously absorbed, instead of one. Afterwards, the electron relaxes and moves to a lower vibrational sublevel. After some time the electron falls back to the ground state by emitting a photon. Image taken from cleogels2010.blogspot.nl[5]

material, they can be absorbed by one of the substance's orbital electrons. The energy of the photon then excites the electron, which means the electron moves to a higher quantum state. After some time, the electron relaxes to the ground state by emitting a new photon with less energy. This new photon has less energy, because the electron loses some energy by non-radiative relaxation before falling back to the ground state. The difference in energy between the absorbed and emitted photons is called the Stokes-shift, named after the earlier mentioned discoverer of the phenomenon.

Fluorescence is shown schematically in the left panel of figure 1. This figure shows a Jablonski diagram which illustrates the excitation and relaxation of the electron after the absorption of the photon. In this diagram, the excited and ground state are represented by horizontal lines. The arrow between these two states illustrates the excitation of the electron after absorption of the photon. Afterwards, the electron moves to a lower quantum sublevel by non-radiative relaxation[2]. This is represented by the small arrow coming from the excited state. Finally, the electron relaxes to the original ground state by the emission of a photon, shown by the downward pointing arrow and the green wave. Many natural compounds exhibit fluorescence, and these compounds are called fluorophores. The wavelength of the emitted photon is characteristic for the electron's quantum energy level and hence for the fluorophore the electron is part of. As a result, different fluorophores will emit photons of different wavelength. This means fluorophores can be detected and distinguished by measuring the wavelength spectrum of the photons they emit. In the experiment, samples containing fluorophores are exposed to light and the resulting fluorescent signal is collected. Then, this signal can be analyzed to detect the different fluorophores present in the sample, because every fluorophore has a distinct fluoroscence spectrum.

The energy of a photon is inversely proportional to its wavelength; lower wavelengths have a higher energy than higher wavelengths. In the visible spectrum, lower wavelengths are seen as blue light, and higher wavelengths appear as red light. The fluorescence discussed so far involved the absorption of a singe photon. Usually, the absorbed photon must posses an energy near the ultraviolet part of the electromagnetic spectrum in order to excite

[2]non-radiative relaxation is the collective name for all the processes where excited electrons lose energy without the emission of photons.

an electron. However, it is also possible for an orbital electron to absorb two less energetic photons simultaneously to acquire the energy needed. This process is illustrated in the right panel of figure 1. The fluorescence involving the simultaneous absorption of two photons is properly called Two Photon Fluorescence (TPF) and it's the type of fluorescence used in the experiment. The energy required per photon is about half the energy of the excited state which allows fluorescence to also occur using a (infra)red light source. The electrons in this experiment are excited using a short-pulse laser which emits a wavelength of 755 nm, which is near the infrared.

Both Two Photon- as Single Photon Fluorescence can be used to generate images. This is done by having a photon beam scan through a specific area of interest while collecting the emitted photons due to interaction. Afterwards, the data can be plotted as an image. In microscopy, imaging using Two Photon Fluorescence Microscopy has two major advantages over fluorescence microscopy with single photon excitation. The first advantage is the fact that (infra)red photons penetrate tissue better than ultraviolet photons[6]. This means TPF microscopy can reach a higher sample dept, allowing for the possibility to scan a deeper area of interest. The second advantage arises from the fact that the chance of two photons interacting with the same electron simultaneously is very low. TPF usually is a quite uncommon process and only at a very high photon flux does TPF become probable. This becomes visible when the photon beam is focussed at the area of interest, which is needed to get a clear image. Fortunately, focusing the beam increases the photon flux: only in the focus is the photon flux high enough for the two-photon fluorescence to take place at relatively high amounts. Away from the focus the flux is too low and virtually no fluorescence takes place. On the other hand, single photon fluorescence has much higher odds of occurring and consequently takes place in the entire depth of the sample. This results in unwanted absorption from regions one's not interested in. This out-of-focus excitation is drastically lowered in the case of TPF. Moreover, the energy of one high wavelength photon is not high enough to cause single photon fluorescence. This means the data will come from a specific area of interest and not from everything in front or behind it. The advantage of TPF over single photon fluorescence is illustrated in figure 2. Conclusively, the result of TPF is a two-dimensional plot where the image depth can be relatively precisely determined and where noise from other regions in the tissue is minimized. This means TPF also allows for three dimensional imaging by systematically changing the focus depth and combining the individual results.

There exists a limit on the total amount of photon collisions a molecule can take before it gets permanently damaged. Even if the molecules do not absorb the photons, they will still collide with them and after a certain time, the molecule will break apart. This photochemical destruction of fluorophores is called photobleaching. Not only the fluorescent materials disappear over time; the chemical makeup in the sample will change as well because all molecules are affected; fluorophore or not. Eventually, this will make the sample unable to represent a natural state and it becomes unusable. With TPF, the photons will have a lower energy and this greatly reduces the photobleaching in the tissue. If the setup will be used on living humans in the future, there might be a chance that this photobleaching alters important molecules inside the body cells. For example, photobleaching can cause mutations in the DNA, which can be very dangerous for the patient. Fortunately, recent research has shown that this phototoxicity in human cells is marginal even compared to sunbathing (Nadyarnykh & Thomas (2012)[7]).

## 2.2 Second Harmonic Generation

The second imaging technique used in the experiment is an effect of directing a photon beam at samples containing materials with nonlinear properties. In electrodynamics, the polariza-

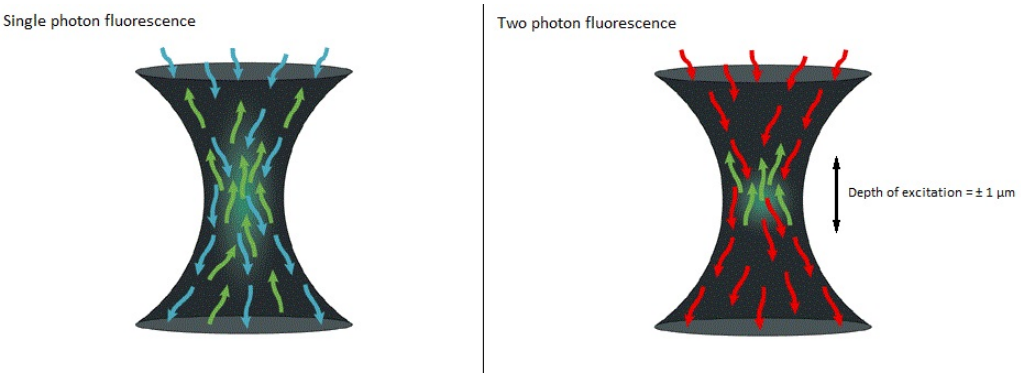


Figure 2: The out-of-focus excitation is drastically lowered using TPF (right) compared to single photon fluorescence (left), because TPF only occurs at high intensity. These intensities are only reached in and near the focus of the photon beam[6]

tion of a material is a function of the electric field[8]:

$$\vec{P}(\vec{E}) = \chi^{(1)}\vec{E} + \chi^{(2)}\vec{E}^2 + \cdots \quad (1)$$

Here, $\vec{P}$ is the polarization, $\vec{E}$ is the electric field as a result of the photons passing through the materials and $\chi^{(n)}$ are dimensionless coefficients where $\chi^{(1)}$ is known as the electric susceptibility of the material. The linear term $(\chi^{(1)}\vec{E})$ is responsible for absorption, scattering and reflection of light. In most cases this term dominates, because $\chi^{(2)}$ is magnitudes smaller than $\chi^{(1)}$. However, the quadratic term can become significant if a material possesses a relatively large nonlinear term. If, in this case, the strength of electric fields (photon flux) is high enough, nonlinear effects can arise and one of these effects is called Second Harmonic Generation (SHG). In this process, pairs of photons interacting with the nonlinear material are "combined" to form one photon with half the wavelength of the original two photons. This process is sometimes used to make near-infrared photons visible to the human eye (figure 3).

Most photons undergoing Second Harmonic Generation will pass through a sample, but a small percentage of the photons is scattered backwards and this signal can be detected. Fortunately, the signals resulting from TPF and SHG are distinguishable: firstly, the wavelength of the photons resulting from SHG can be predicted; they will have exactly half the wavelength of the photons in the laser pulse. Secondly, the width of the spectral peak of the SHG is in the same order as the laser, because no additional spreading arises in the process. TPF spectra, on the other hand, has a much wider peak: quantum energy levels consist of minor vibration sublevels, with slightly different energies (figure 4). As a result, the energy difference between the excited and the ground state can vary. Furthermore, the amount of energy loss by non-radiative relaxation isn't always equal. Consequently, the light emitted as

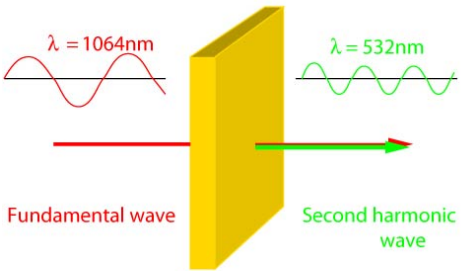


Figure 3: An infrared beam of light moves through a nonlinear material. Pairs of the infrared photons with a wavelength of 1064 nm are combined and form single photons with a wavelength of 532 nm (green light)[9].

a result of TPF, will have wider spectrum than the spectrum of the laser, as shown in figure 5. Consequently, the photons resulting from SHG can be recognized by their narrow peak. This gives the possibility to discriminate the signal from Second Harmonic Generation from the signal resulting from Two Photon Fluorescence, meaning both can be used in the experiment.

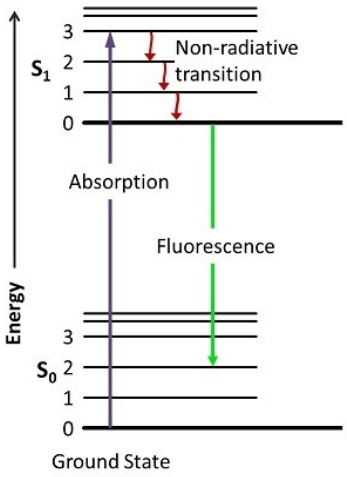


Figure 4: Due to quantum sublevels, the energy difference between the ground state and the excited state can vary[10]

## 2.3 Tumor cells and metabolism

The goal of the experiment is to find a way to detect cancer cells using the previous mentioned TPF and SHG. Cancer is an illness where body cells diverge from their regular life cycle: during an animal's life, cells grow and divide at a controlled phase. Old or damaged cells die and are replaced by new ones: this is their regular life cycle. However, sometimes the DNA of a cell becomes damaged or changed, producing mutations that affect normal cell growth and division. When this happens, cells do not die when they should and they form new cells at a hastened rate. Cells with these type of mutations are called

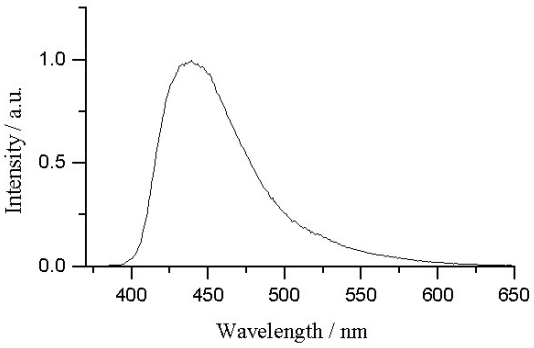


Figure 5: A typical spectral graph resulting from TPF. In this diagram, the horizontal axis represents the wavelength of the photons and the vertical axis represents the intensity. Conclusively, the spectral graph shows the photon flux per wavelength. This specific graph shows that the TPF spectrum contains a relatively broad peak with a 'tail' towards the higher wavelength[11].

cancer cells, and they are characterized by an unusual long lifespan and by an increased and unregulated cell division rate. This divergence from healthy cells can be seen back in the cell's metabolism (the totality of the cells vital chemical processes).

The setup will use changes in the cell's metabolism to detect cancer cells in animal tissue. Many molecules in living tissue are known fluorophores, leaving many possibilities to detect changes. This natural emission of light by biological structures is called autofluorescence. One of these molecules is the coenzyme Nicotinamide Adenine Dinucleotide (NAD+). One of NAD+'s roles in a cell is the transfer of electrons from one chemical reaction to the other[3]. It accomplishes this by accepting electrons from other molecules, forming NADH. Afterwards, NADH and oxygen can react to reform NAD+, releasing the previous accepted electron elsewhere. The resulting NAD+ can then be re-used. However, in cancer cells oxygen is less abundant: cells get their energy from oxygen and cell

division costs energy. Consequently, cancer cells use more oxygen for their accelerated cell division slowing down other oxygen dependent processes like the (re)formation of NAD+. As a result, cancer cells possess a larger amount of NADH compared to healthy cells. Because NADH is a fluorophore, it can be detected using TPF microscopy, as is shown by Palero (2011)[12].

Animal tissue contains nonlinear materials as well. An important one is called Collagen and it is in many animals, a very abundant protein. Collagen is found within the Extra Cellular Matrix (ECM), which is the name for structures inside animal tissue but outside the cells. Research by Jones et al.(1980)[13] has shown that cancer cells can digest parts of the ECM, including Collagen. Using Second Harmonic Generation, the abundance of collagen can be detected and can be utilized as an extra method to detect cancer in tissue.

After the experiment, it will be made clear if the setup can be used to identify tumors in mice tissue. If this is the case, further steps can be made for the development of an useable medical device based on this principle for use in hospitals on real patients.

# 3 Instrumentation

The theory outlined in the previous chapter can be utilized to detect tumor cells in animal tissue: mutated cells have a distinct metabolism and the differences can be detected with Two Photon Fluorescence- and Second Harmonic Generation microscopy. In the setup, this theory is brought to practice. A schematic illustration of the setup is shown in figure 6. Here, different optical devices are labeled from 1 to 9. In the following paragraph, a short outline of the setup is given.

In the setup, a laser is used as the photon source. In figure 6, the laser is labeled (1) and the arrow pointing out of the laser represents the laser beam. After emission, this beam proceeds through a number of optical devices (labeled $2, 3, 4, 5$) that optimize the beam for imaging. These devices will be discussed in more detail in this chapter. Afterwards, the beam enters a fiber at the fiber launcher (7) which leads to a scanner. The scanner ends in a probe and here the photons leave the setup to interact with a sample, placed under the probe on the microscope stage. The photons emitted by the sample as a result of TPF and SHG re-enter the setup through the probe and the fiber. This means that during a measurement, two signals are passing through the fiber in opposite direction: the photons from the laser pulse moving to the sample and the emitted photons coming from the sample. These two signals are discriminated at the dichroic mirror (6). This mirror lets the incoming laser beam pass, but it will send the data beam coming from the fiber to the two detectors $(8, 9)$. After detection, the data is send to a computer and stored on the hard disk. Then, image processing software called ImageJ is used to open the data files and to generate images and spectra which can be analyzed. More detail on the image processing software and the data analysis will be given in a later section.

The setup was built in Utrecht, but it has been moved to Erasmus Medical Center (EMC) in Rotterdam. Permission is needed for the use of mice in the experiment and the Committee

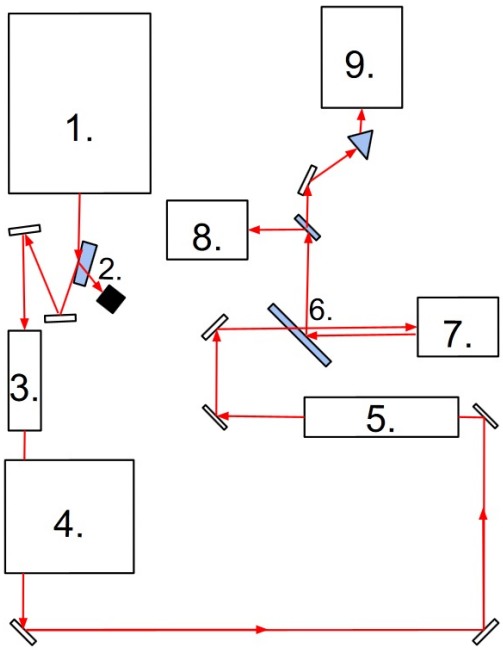


Figure 6: An schematic outline of the setup. The laser (1) emits a laser beam which proceeds through a number of optical devices (labeled $2, 3, 4, 5$) that optimize the beam for imaging. Then the laser beam is used for TPF and SHG at label 7. Afterwards, the resulting signal proceeds to the detectors $(8, 9)$

on Animal Research of the EMC has approved the experimental protocol. The entire setup is located on a mobile $0,6 \times 1,5$ m table. Environmental light will disturb imaging and to keep it away from the setup and the detectors, a cover has been made and installed on top of the table by the department experimental medical instrumentation within the EMC. This cover also prevents direct exposure to the laser, which can severely damage eyes. The cover consists of an inner and an outer part. The inner part is made out of anodized aluminium and it covers the laser output and the first four optical devices in figure 6. In this part of the setup, the laser's power is very high and can damage the outer part of the cover. Aluminium is a good heat conductor, so an out of place laser beam won't burn through it.

The outer part of the cover encloses the entire setup with black plastic. The laser beam will lose power while passing through the different optical devices of the setup and after the fourth device, the plastic won't be damaged by the laser beam. The outer part of the cover also keeps environmental light away from the remaining setup. Figure 7 shows the setup in its cover[3].

The mirrors and optical devices have to be

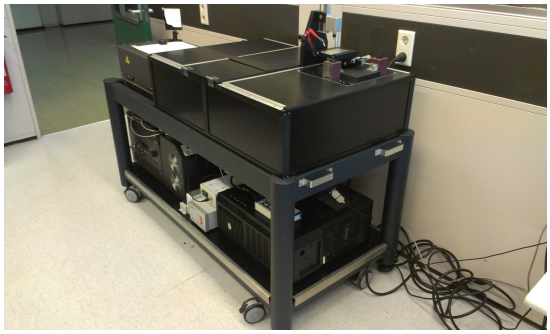

Figure 7: The entire setup is located on the $0,6 \times 1,5$ m mobile table. The outer part of the cover made out of plastic encloses all optical devices. The hinges of the doors that allow easy access to a part of the setup, can be seen on the top-left side of the cover. Underneath the table, a computer is located which is used to control the imaging. The laser used in the experiment can be identified by the yellow warning symbol.

carefully aligned: daily temperature changes alone are enough to disrupt a correctly aligned setup making accurate measurements impossible. Consequently, re-alignment is needed every day or for certain parts; every few hours. To make alignment possible, doors are installed at the top of the cover which allow access to the setup at the places where alignment is needed frequently. Furthermore, the entire top of the cover can be completely removed if adjustments in others parts are required.

In the following subsections, each of the optical devices illustrated in figure 6 is discussed in detail.

[3]An earlier image of the setup with all the optics visible can be found in the appendix.

## 3.1 Laser

The laser (Labeled 1) used in this research is a Coherent Inc. Chameleon Ultra II Titanium Sapphire Laser (Ti:Sa Laser). The laser emits short (140 fs[4]) pulses of photons with a repetition rate of 80 MHz. There are two reasons why a pulsed laser is used instead of a continuous beam: firstly, the peak power of a pulsed laser beam is much higher than the intensity of a continuous beam with constant power. This is caused by the short duration of the pulse: the same energy is outputted in short intensified bursts, leading to a high photon flux. This peak power is needed for TPF: as said in the previous section, simultaneous absorption has low odds of happening and consequently only occurs measurably at high photon intensities. Secondly, the relatively long intervals between the pulses (order of $10^6$ times larger than the pulse length) give the laser time to lose the generated heat more effectively. This is better for the laser and it allows for longer periods of continuous activity.

The wavelength of the laser beam can be set to values between 680 and 1080 nm, and in the experiment a wavelength of 755 nm is used. Usually, a laser will be almost perfectly monochromatic, meaning its emitted beam will have a minimal spread in wavelength with a variance of only $10^{-3}$ nm. However, due to the very short duration of the pulses in the experiment, the spread in wavelength is increased to a variance of $\pm 5$ nm. This is unfortunate, but it's more important to keep the pulse length very short for the high peak intensity.

The laser's power is set to its maximum of $4,0$ W, which is done because the laser preforms best at its highest power. However, this power is generally too high for the optical items used in the setup. To prevent the different mirrors, lenses and grating from being damaged, the power is brought down to 32 percent by a wedge placed in front of the laser (Label 2 in figure 6). The larger part of the laser beam will pass through the wedge undergoing refraction, and ends up in a beam dump. The other fraction reflects and is used for the imaging. The remaining power of the laser is $1,3$ W.

[4]here, the pulse length is defined as the full width at the half maximum (FWHM)

## 3.2 Beam expander

After the wedge, the intensity may still be too high for the optics in the experiment. However, the laser will already lose a large portion of its power while passing through these optics bringing down the power more is unfavorable. To lower the intensity without losing more power, a beam expander is used (label 3 in figure 6). This device increases the surface area of the laser pulse, effectively lowering the intensity. The beam expander utilizes two lenses with different vocal lengths (30 mm and 100 mm respectively). By making the distance between the two lenses equal to the sum of the two focal lengths, the laser beam will be broadened and parallel after passing through the device.(figure 8). In the focal point of the beam

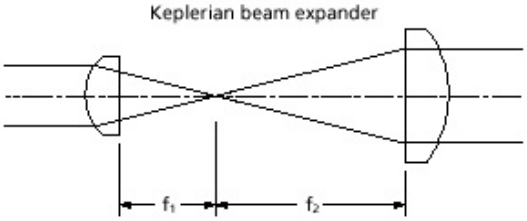


Figure 8: The beam expander utilizes two lenses with different focal lengths. The distance between the two lenses is equal to the sum of the two focal lengths[14].

expander, a pinhole is placed to remove unwanted reflections and higher order transferal modes. After the beam expander, the power of the laser beam is $0,49$ W. This power loss is inevitably caused by the pinhole and imperfections in the setup or by environmental factors. Consequently, the laser beam will lose power passing through the various optics in the setup as mentioned earlier.

## 3.3 Group velocity dispersion compensator

When light travels through a medium, photons with higher wavelengths often have a slightly higher group velocity than photons with lower wavelengths. As a result, the length of the laser pulse is gradually broadened while passing through the setup, with the higher wavelength photons traveling ahead of the photons with relatively lower wavelength. The broadening of a light beam is called dispersion. Fortunately, in most of the setup the light travels through air where the pulse broadening is is minimal. However, in the fiber(part of label 7 in figure 6) which is made of fused silica, the dispersion is significant. While the spectral peak of the laser pulse is narrow (10 nm), the extremely short pulse length of the laser causes the dispersion to have a relatively large effect: without corrections, the pulse length will, theoretically, increase from 140 to 790 fs[5] This is problematic, because this broader pulse has a much lower peak intensity.

The dispersion of the laser pulse is compensated by the Group Velocity Dispersion Compensator (GVDC, 4 in figure 6). The GVDC consists of two gold plated gratings: the first grating splits up the different wavelengths, while the second one re-combines them. Between the two gratings, photons with higher wavelength travel slightly longer distances than photons with shorter wavelength. Consequently, the photons with shorter wavelength have a head start when the laser pulse enters the fiber. This way, the dispersion occurring in the fiber is compensated. However, the GVDC can only compensate for first order dispersion and while this type of dispersion is dominant in the fiber, higher order dispersion effects are still present. Consequently, it is impossible to completely compensate for the dispersion and the final pulse length, with use of the GVDC, will be 200 fs. While this is still a higher pulse length than the 140 fs of the original beam, it is short enough for imaging. After the GVDC, the remaining power of the laser beam is 0,35 W: the gratings reflect the laser pulses in multiple orders and only the negative first order is used in the remainder of the setup containing about 80 percent of the reflected photons.

[5] see the appendix for a short derivation of this value.

## 3.4 Spatial mode filter

The photon intensity of the laser beam has a distinct pattern in the plane perpendicular to its propagation direction. This pattern can contain multiple nodes and anti-nodes and it is called the spatial mode of the laser beam. Usually, the spatial mode is a superposition of multiple individual modes, where every mode is a possible solution to the Maxwell equations. If an electromagnetic wave contains only a single of these modes, the wave is said to be 'single-mode'. A number of single-modes for rotational symmetric boundary conditions are shown in figure 9.

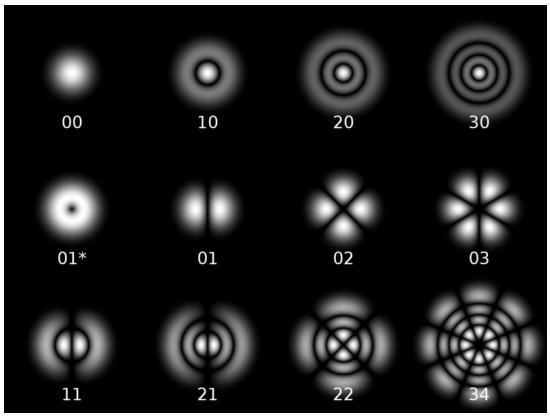


Figure 9: The first few cylindrical modes of a transverse electromagnetic wave[15].

As mentioned earlier, two signals have to pass through the fiber when the setup is active. The laser beam in one direction and the TPF and SHG signal in the other. This is only possible if the laser beam is single-mode, because this allows the the signal to pass through a different part of the fiber than the multi-mode TPF and SHG signal. To obtain the required single-mode laser beam, a spatial mode filter (label 5 in figure 6) is used. This filter will absorb all spatial modes but one and as a result

the remaining laser pulse will only contain the transmitted mode. Unfortunately, the absorption of all other modes drastically lowers the laser's power and after passing through it, the remaining power of the laser beam is just 0,15 W

## 3.5 Fiber

After the laser pulse has been properly adjusted, it will be led to the scanner by a double-clad photonic crystal fiber. 'Double clad' means the fiber possess three layers of optical material instead of two: it consists of a single-mode core, surrounded by both an inner and an outer multi-mode cladding each made out of pure silica[16] (figure 10). The core of the fiber is located in the center (diameter: 16 $\mu$m), while the inner cladding can be identified as the part of the fiber containing tiny black dots surrounding the core. These dots are air holes, and they're used to realize the required refraction index. The outer cladding starts at an average diameter of 163 $\mu$m, just outside the hexagram containing the air holes. The thick black ring surrounding the three layers is a coating, preventing the light from escaping the fiber.

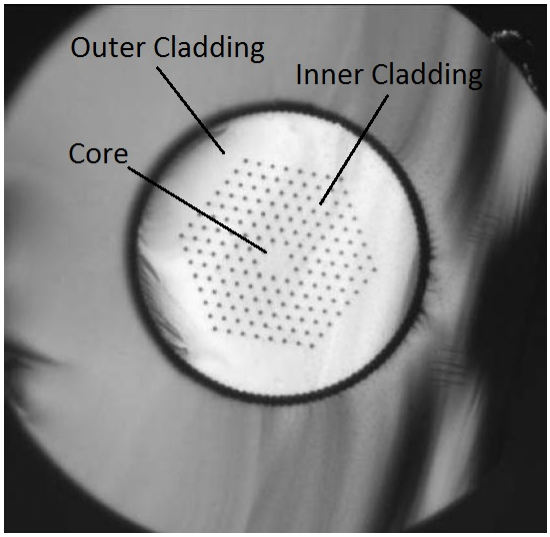


Figure 10: a cross section of the fiber where its tree layers and its coating are visible. The core of the fiber is located in the center (diameter: 16 $\mu$m), while the inner cladding can be identified as the part of the fiber containing tiny black dots surrounding the core. The outer cladding starts at an average diameter of 163 $\mu$m, just outside the hexagram containing the air holes. The thick black ring surrounding the three layers is a coating.

This fiber has been manufactured to allow for a two-way signal: the single-mode laser signal traveling forward, and the emission data signal traveling in the opposite direction. A fiber is chosen, because it allows the scanner's position to be adjusted within a certain limit which is necessary to properly place the scanner in front of the sample. The fiber has a length of 1 m. The fiber is coupled by an objective lens (Nikon S Fluor; 20x, NA 0.75). Without it, the surface area of the laser pulse would be too large to enter in the fiber completely.

## 3.6 Scanner

The scanner is the device located at the end of the fiber and it is where the laser pulse is coordinated toward the sample. It is waterproof, lightweight, compact and has been developed by Philips©(figure 11). In the scanner, the light is focussed using a single element a-spherical lens with a diameter of 1 mm (0.6 NA). After being focussed, the laser pulses leave the scanner through a long, 3 mm thick probe. The narrow size of the probe makes it possible to insert the scanner in living tissue with minimal tissue desecration. The probe is directed using coils that drive magnets attached to the fiber. The position of the probe can be adjusted in two dimensions independently by increasing or decreasing the current going through the respective coils. The third dimension can be adjusted by adjusting the height of the scanner. During a measurement, the scanner will use the coils to lead the probe (and thus, the laser pulse) pixel by pixel in a pattern which covers the entire area of interest, roughly 140 by 140 $\mu$m in size, while the setup collects the excitation spectra. During the scan of a pixel, the TPF

and SHG signals are captured via the probe and led back to the setup through the fiber.

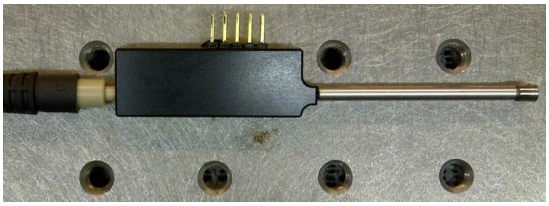

Figure 11: The scanner used in the experiment. It is compact, lightweight and waterproof. The probe has a diameter of 3 mm. The distance between the holes in the table is 25 mm. Image taken from Alkemade (2012) [17].

The scanner is intended to scan in a spiral pattern and the software included is designed to work in this pattern. During a spiral scan, the scanner starts in the middle of the area of interest and then spirals outwards during the scan to create an image. Another option is to start on the edge of the area and then spiral inwards. The spiral can be very practical, because it allows the scanner to move at a constantly increasing or decreasing speed without sudden shifts in direction or velocity. Furthermore, its pattern is created relatively easy by letting the current passing through the coils follow harmonic functions, as illustrated in the top of figure 12. Here, the blue and red lines stand for the currents going through the two coils representing the two dimensions of a two-dimensional scan. The two waves are $\frac{1}{4}\pi$ out of phase, creating a circular pattern. The slowly decreasing amplitudes then creates the spiral pattern.

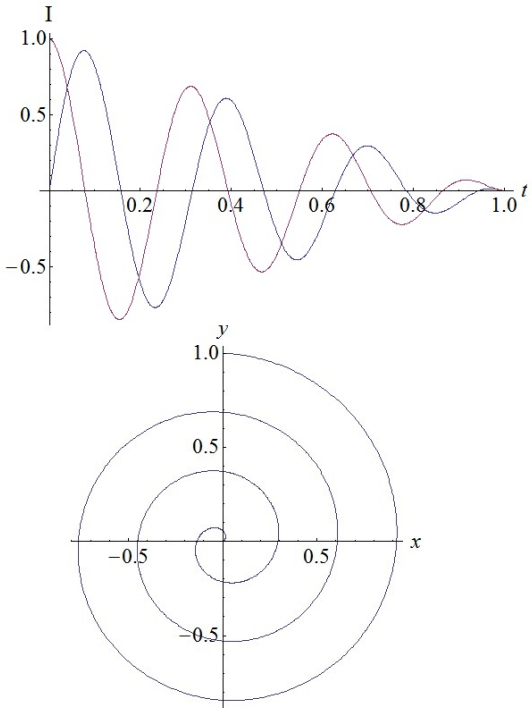


Figure 12: Top; the current going through the coils as a result of the oscillating voltage. The two waves are $\frac{1}{4}\pi$ out of phase and their amplitude lowers linearly. Bottom; the resulting pattern the scanner will follow. The values shown are standardized and do not necessarily coincide with the actual currents. Note that the image is exaggerated for clarity and that the circle density is much higher in the actual pattern.

While scanning in a spiral pattern is the intended type of scanning, it also has some significant disadvantages. Firstly, image processing software usually works with raster images where the pixels are on a two dimensional rectangular raster or grid. Any regular image file found on a computer is saved in this format. To open the data resulting from the spiral scan, it first has to be converted to a raster image. Converting is always bad for image quality and besides that, it is unpractical to have to convert every data file. Another disadvantage comes from the fact that the camera detects at a constant speed. According to figure 12, the period of the two oscillation voltages remains constant while the amplitudes decrease. As a result, the scanner spirals inwards at a constant rate while the radius of the spiral pattern decreases continuously. This means that after every period, the scanner will have traveled a smaller distance (smaller circle) in the same time (constant period).

Conclusively, the scanner's velocity decreases during the scanning process. Because the camera takes the same amount of pixel every circle, the pixel density in the middle of the image (low scanner speed) is higher than on the edge of the image (high scanner speed). To correct this issue, the frequency of the alternating voltage can be increased while the scanner moves outward. However, this changes the relative ease of spiral scanning, as careful adjustments are necessary. What is more, the scanner used in the project vibrates in or near one of its resonance frequencies. The system has the preference of staying into this resonance, making adjustments in the frequency unpractical.

Due to the disadvantages of the spiral scan, mentioned in the previous paragraph, the scanner has been programmed to follow a raster scan instead. This removes the need for conversion and if adjustments in the voltage pattern are required after all, it might as well be changed to a raster pattern. This pattern is shown in figure 13, top. To generate a raster pattern, one of the voltages is increased and decreased linearly and periodically resulting in a triangular form, while the voltage controlling the second dimension must increase in linear steps during the scan. Combined, they make the pulses moves in a zigzag pattern forming a raster (figure 13, bottom.)

The raster scan is nice, but in practice, it is not perfect. One issue occurs near the sides of the image, where the scanner reverts. Mechanically, the scanner cannot revert instantaneously and it will slow down first before it accelerates in the opposite direction. Conclusively, the tips of the triangles in figure 13 are slightly rounded. As previously mentioned, the camera has a constant detection speed and the software places each pixel assuming a constant velocity. This means the pixels near the edge will not represent what the software thinks they will, resulting in unusable data. Moreover, raster scanning is not supported by the standard scanner software, and thus custom software must be written. This is done in LabView. The software used in the experiment will be discussed in greater detail later in this thesis.

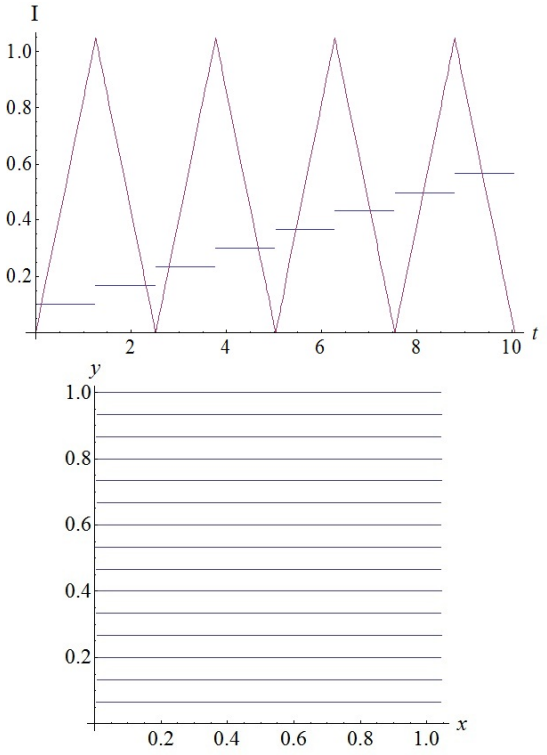


Figure 13: Top; the current going through the coils as a result of the voltages needed for raster scanning. One follows a periodic triangle, the other increases in linear step. Bottom; the raster pattern the scanner will follow; the scanner starts in the top left corner and moves to the right. At the end of the line, the scanner moves down a line and returns to the left, resulting in a zigzag pattern. The values shown are standardized and do not necessarily coincide with the actual currents.

## 3.7 Animal model and the microscopic plate

To determine whether nonlinear imaging techniques like Second Harmonic Generation and Multi Photon Fluorescence can be used *in vivo* as a reliable optical diagnosis, the setup will scan the skin of living mice in a period of 8 weeks. These mice are hairless and bred in het Erasmus Medisch Centrum Rotterdam. For a

period of 12 weeks, before and during the experiment, a specific tumor generating mixture of chemicals is applied on their backs. The mixture consists of two chemicals which are 7,12-Dimethylbenz(a)anthracene (DMBA) and 12-O-Tetradecanoylphorbol-13-acetate (TPA). DMBA is a powerful laboratory carcinogen and it causes the mutations in the cell-DNA that cause tumor growth[18]. TPA then helps the emerged mutated cells to survive and expand in number[19], promoting tumor development.

On the skin of the mice, certain areas will be marked and these marked areas will be scanned multiple times during the emergence and growth of the tumors. This way, it can be established how the two imaging techniques work in different stages of tumor development.

During a measurement, it is important that the mice do not move. Because the scanned area is relatively small, even the slightest movements cause big distortions in the images. Therefore, the mice are anesthetized and placed on a heated microscopic plate so they stay at a constant temperature of $37^o$. This is also the reason the tumors are being developed on the back of the mice. During breathing, the back of the mice won't move nearly as much as other parts of the body like the stomach or the chest. The heated microscopic plate has two degree's of freedom so it can be positioned correctly under the scanner. An image of the microscopic plate under construction is shown in figure 14.

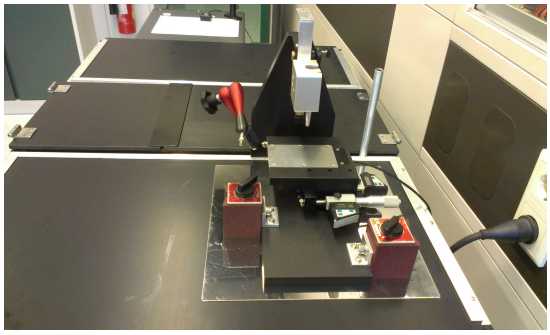

Figure 14: An image of the microscopic plate under construction. The plate has two degree's of freedom and will be held at a temperature of $37^o$. Note the doors located on top of the cover.

## 3.8 Dichroic mirror

As mentioned in the introduction of this chapter, the dichroic mirror splits the laser pulses moving to the fiber from the TPF and SHG signal coming from the fiber. This is illustrated in figure 15. The dichroic mirror transmits light up to a wavelength of 735 nm, while photons lower wavelength are reflected. Conclusively, the photons with a high energy are reflected and below a certain energy (higher wavelength), all photons are transmitted. The photons of the laser pulse have a high enough wavelength and are transmitted. SHG on the other hand, halves the wavelengths of absorbed photons doubling their energy. As a result, the photons from SHG are reflected by the dichroic mirror after passing through the fiber. The same holds for TPF. The emitted photons resulting from TPF have a higher energy than the absorbed photons from the laser and therefore, the TPF signal is reflected as well. By placing the mirror at an $45^o$ angle, reflected photons make a right angle directing them to the two detectors.

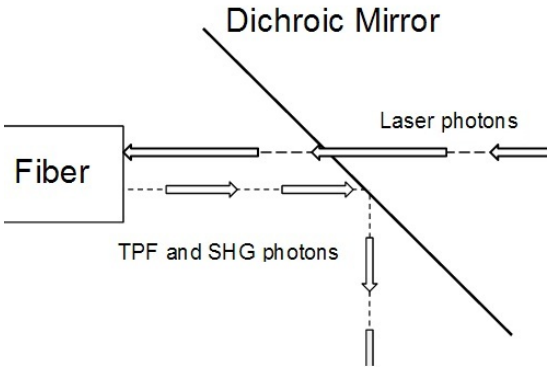


Figure 15: This figure shows the role of the dichroic mirror in the setup. The photons from the laser are transmitted and enter the fiber while the SHG and TPF photons from the fiber are reflected at a $90^o$ angle, directing them to the detectors

## 3.9 Detectors

### 3.9.1 photomultiplier detector

After being reflected, the data signal progresses towards the detectors. Using a flip mirror, the signal is send to either one of the two detectors. One of these is a photomultiplier tube (PMT). The PMT is a detector which can measure photon intensity. In the experiment, the PMT detector is mostly used for alignment: before the scanning begins, it has to be made sure the scanner is correctly focussed. The PMT can used to focus the scanner, because it will receive a high signal at a correct focus. After the focus is correct, the flip mirror is turned so the excitation signals are send to the other detector; the CCD camera.

### 3.9.2 CCD Camera

The second detector in the setup is a an Andor iXon3 860 Charged Coupled Device (CCD) camera. In front of the camera, a prism is placed to separate the photons with different wavelength, as illustrated in fig 16. Afterwards, the camera uses 128 light sensitive channels to divide the spectrum in 128 sets of wavelength to detect the separated photons individually within a specific wavelength range. As a result, the CCD camera can obtain an intensity per wavelength range per pixel. This means 128 data values are received per pixel. Besides the SHG and TPF signals, the camera also detects the present background signal. The resulting background spectrum can later be subtracted to get rid of the environmental noise in the data. During a measurement, the data of the measured values is send directly to a computer. The computer receives 128 data values per pixel plus another 128 data values for the background spectrum, resulting in a total of 256 values. To summarize the scanning process: when a scan is initiated, the probe of the scanner starts moving in the raster pattern, directing the laser pulse pixel by pixel over the entire area of interest. For every pixel, the emitted photons are captured by the probe and send to the camera which detects the intensities and the background for each set of wavelengths. This process continues until the probe has completed its pattern and has scanned all pixels. The camera sends the data directly to a computer where it is stored on a hard disk. Then the data can be analyzed.

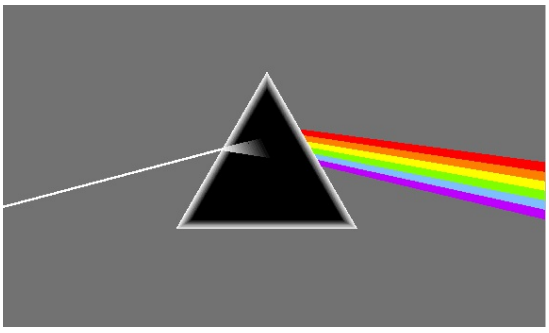

Figure 16: Because the refractive index of the prism depends of the wavelength, the refraction occurring in a prism separates a light beam in its independent wavelengths[20]

# 4 Data acquisition

The goal of a setup is to receive useful data from it. In order to successfully acquire data, the setup has to be properly controlled and the data has to be correctly collected. Small errors or misalignments in either, or between these processes may cause completely distorted images which are useless. Solid programming is required to make sure everything is doing what it's supposed to at the correct time. In this section, the different software used in the experiment are discussed in more detail.

## 4.1 National Instruments box and LabView

As previously mentioned, the scanner's standard software doesn't support scanning in a raster pattern. Therefore, custom software has been written in a data acquisition program called LabView. National Instruments' LabView is used to control both the scanner and the camera rather than the software developed by their respective manufacturers. This is done because synchronization between the two devices is easier realized within one program and the scanner required custom software in any case. In the LabView UI, users can set options like the size of the scanned area and the resolution of the image. During a measurement, LabView drives the scanner in the correct pattern, while it collects data from the camera. After a scan, LabView can export the data and save it as a .spe file on a local hard drive.

To connect the computer running LabView to the different instruments, a LabView box and a digital acquisition card are used. This card is placed in the desktop case and is at one side installed to the computer's motherboard. The other side of this piece of hardware contains an output port, which can be connected to the box by using a specific cable. The LabView box posses all the in- and outputs required to connect the instruments to the computer and the LabView software recognizes the card if properly installed and can utilize it to control the different instruments.

## 4.2 Data Files

The data in the .spe file created by LabView, is saved as a list of hexadecimal numbers; every 256 numbers represent one pixel of the image: the first 128 stand for the spectral channels from the camera and the second 128 are the respective background signals. Hexadecimal is a numeral system by which values in the system are represented by sixteen distinct symbols. Each hexadecimal number is written using two bytes, where one byte has 128 ($2^8$) possible configurations. Combined, two bytes allow for values between 0 and 65536. In front of the data, LabView places a header consisting of 4100 hexadecimal values. This header contains information about the data file, which is needed to read in the file properly. It contains, among other things, information of the amount of pixels and how many bytes represent one data point. Figure 6 shows a small portion of a .spe file from the experiment.

## 4.3 ImageJ plugin

After a measurement, the resulting data files have to be opened and converted into images and spectral graphs. These images, but especially the graphs, could be used to conclude if the methods used in the experiment are useable for the detection of tumors in organic tissue. It is important the right image processing software is used to assure that correct results are found. For the task of reading and analyzing the data, a program called ImageJ has been chosen. ImageJ is an open source image processing program written in java and it has been chosen for its great flexibility: ImageJ's open source nature and the fact that it has good support for plugins, means it can be adjusted relatively easily for the specific demands of any experiment.

As seen in the previous section, the data is stored in a very raw format: it is basically nothing more than a list of values, from which the first 4100 are a header containing informa-

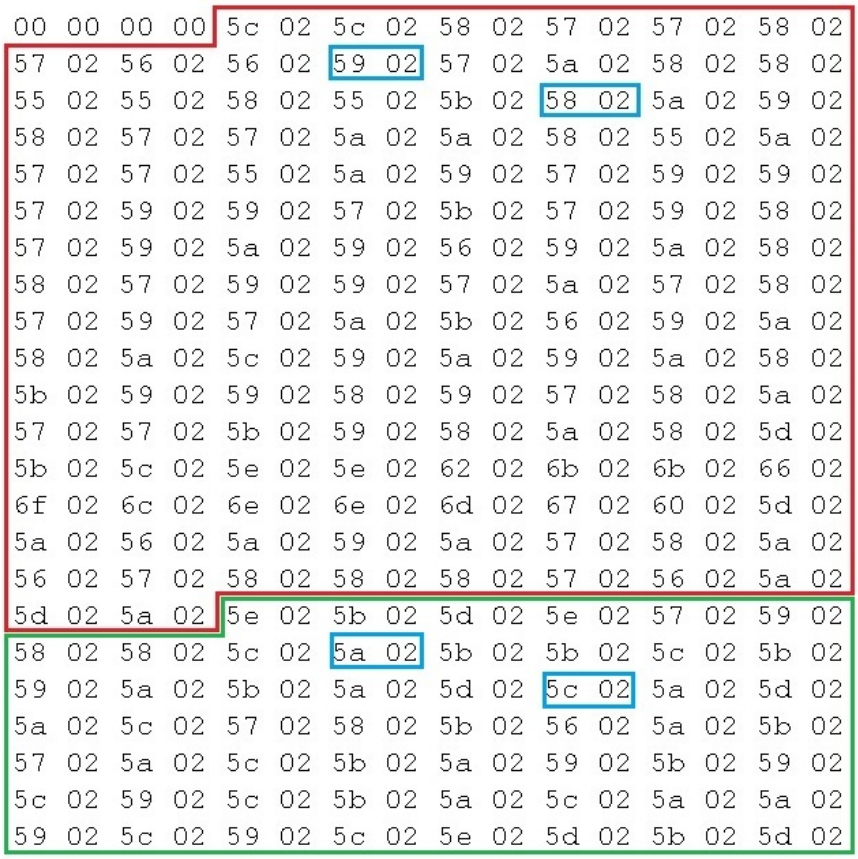


Figure 17: A small part of a data file generated by the experiment. the zero's at the left top corner are the final numbers forming the header. The (hexadecimal) numbers enclosed in red represent the data from the 128 channels for the first pixel where one channel is represented by two pairs of symbols. Of the 128, two random values are marked by a blue rectangle to illustrate what one value is. The numbers enclosed in green form the background signal of the first pixel (not entirely shown). Here, the background values representing the same channel also have the a blue rectangles around them.

tion of the file. ImageJ needs information on how to read the header before it can read the data. More importantly, software is needed to convert the data in the different images and graphs. For these tasks, there exists a plugin for ImageJ within the Molecular Biophysics department of the University Utrecht and it allows ImageJ to open and convert the .spe files.

The plugin has not been written for this experiment specifically. This means the plugin contains more applications than just the ones needed. Consequently, some input is needed to make tell the plugin which applications it has to use. For this puropose, The plugin utilizes a configuration file which is selected (manually) when opening a file. In the configuration file, the plugin is told, for example, that the data is the result of a spectral scan, that there are two lines per pixel and that these lines represent the fore- and background signals respectively. The configuration further allows background substraction to be turned off. This

can be useful during the testing phase of the project because in that case, the background signal can become slightly larger than the data signal. Subtraction will then result in negative intensities at certain pixels.

When a data file is opened with ImageJ, the plugin collects the information contained in the configuration file and the header and uses it to store the data in individual voxels, one per pixel. Afterwards, these voxels can be opened individually and used to construct the various images and graphs. Momentarily, the plugin is used to create four different images and graphs: an intensity image, a RGB image, a spectral diagram and a phasor diagram. What they are and how they can be used will be further discussed in the following subsections.

### 4.3.1 Intensity image

An intensity image is very similar to a digital black-and-white 'picture'. The image is bright where the camera has detected relatively many photons, while the pixels are darker if less photons are detected. The main process involved in the creation of an intensity image, is the conversion from the 128 channels to one value representing the global intensity. To create the intensity image, the voxels created in the plugin are opened one by one and their content is converted to a single value between 0 and 255 to represent the intensity of the pixel. In the image, a value of 255 will translate to completely white while 0 will be totally black. After conversion, this value is given $(x, y)$ coordinates representing a square grid: the first value is placed in the top left corner of the grid $(0, 0)$ and the following pixels are placed right from it $(0, (1, 2, 3, 4, ...))$, until the first line of pixels is complete. Then a new line is started $(1, (0, 1, 2, 3, 4, ...))$ and process repeats until all voxels (pixels) are placed. This pattern is the same as reading a book: a sentence is read from left to right until the end of a line is reached. Then, the text continues in the next line, with a new sentence and so on. However, The pattern in which the voxels are placed, is different from the order the pixels are stored in the data: the scanner has acquired the data in a zigzag pattern, going back and forth through the area of interest. As a result, the even lines $(0, 2, 4, ...)$ are scanned from left to right, while the uneven lines $(1, 3, 5, ...)$ are scanned from right to left. Without adjustments, this means all uneven lines will be placed on the grid in the opposite order, creating a cluttered image. A few lines of script in the plugin are written to solve this problem by changing the coordinates of the values of every uneven line from $x, y)$ to $(Length[x] - x, y)$.

### 4.3.2 RGB image

While an intensity images shows where the largest concentration of fluorophores and collagen are located, it does not distinguish between different substances. The intensity of every spectral channel in one pixel, are combined and converted to a single value: no distinction between channels is made and this results in the loss of spectral information, which is needed to discriminate the different substances that might be present in the sample. For this purpose, a RGB image is generated, which is similar to a digital colour 'picture'. It is created by translating the information of the 128 channels pixels to three values representing the proportion red, green and blue (RGB). These values are then translated to one colour per pixel and put on a grid in the same way as with the Intensity Image.

### 4.3.3 Spectral diagram

The two images described in the previous subsections give a very nice visual representation of the scanned area but for a quantitative analysis, they are not very useful because the spectral information is lost in the conversion process. For actual analysis of the data, a spectral diagram is generated. An example of such a diagram has already been shown in figure 5. In this diagram, the horizontal axis represents the different wavelength and the vertical axis represents the intensity. Consequently, the spectral graph shows the photon flux per photon wavelength. Because the samples contain multiple fluorophores and nonlinear materials, the

resulting emission spectra will be a mixture of the individual spectra. In the analysis, the goal is to discriminate these spectra and see if they coincide with the well-known spectra of the individual substances. This way, the proportions of the different substances in the samples can be derived.

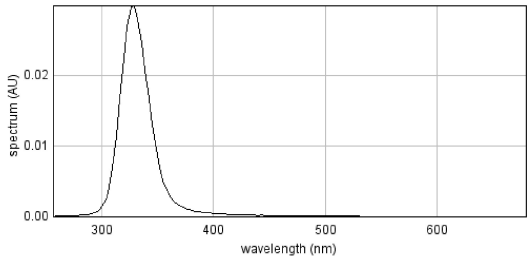


Figure 18: a spectral diagram with a single peak at 325 nm

### 4.3.4 Phasor diagram

An extra data visualization method that can be helpful during quantitative analysis is a phasor diagram. The phasor diagram can help discriminate the different spectral peaks in the spectral diagram as spectral analysis usually requires complex algorithms (typically a least-square fit). Moreover, a relatively large amount manual input is needed and even then, multiple solutions may fit the same spectral diagram. To find the correct solution both easier and more accurately, the phasor diagram can be used.

A phasor diagram is constructed by calculating the fourier transform of the first harmonic of the spectrum, and plotting the real and imaginary part on a graph with an real and imaginary axis. This way, much less input is required by the user and a fourier analysis is completed faster than the time it takes to create a least-square fit. In a phasor diagram, the possible wavelength of the photons are distributed evenly over a circle, much like the straight x-axis of the spectral diagram. Here, a high presence of dots near the edge of the circle represents a high photon flux at that wavelength. This is illustrated in figure 18 and figure 19. The single peak in spectral graph in figure 18 coincides with the spot made of the coulored dots in the phasor diagram of figure 19. Figure 20 shows how the phasor diagram helps finding the different spectral peaks that make up the spectral graph of an image.

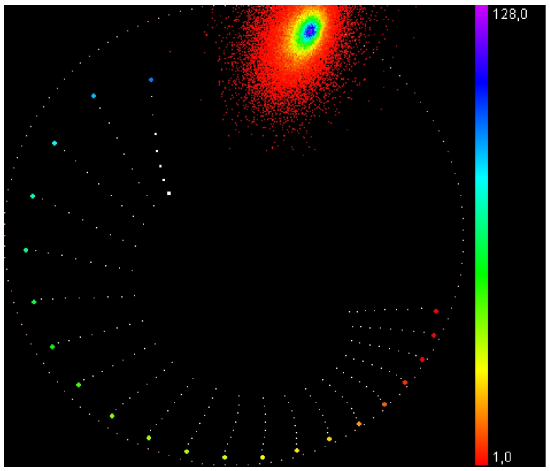


Figure 19: A phasor diagram of the same data as figure 18. Just as in the spectral diagram, the phasor diagram shows a single peak (spot) near the blue side of the visible spectrum.

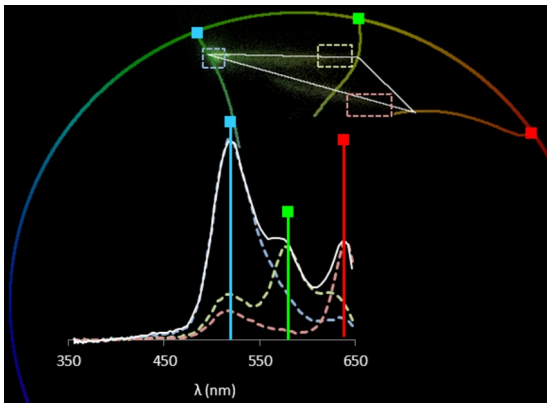


Figure 20: In this figure, one can see both the spectral image and the phasor image of a spectral scan. In the phasor file, the spectral peaks can be identified and used for the spectral analysis. Image taken from F. Fereidounie (2012).[21]

# 5 Results

Once the 12 week period is set in motion and the mice are bred and exposed to the chemicals, it is impossible to pause the experiment: the plan is to follow the tumor development which cannot be stopped halfway. Furthermore, the mice usually will not survive much longer after these 12 weeks. Consequently, it has to be made sure the setup works accurately and consistently before the mice program is commenced. To guarantee this, an extensive testing phase is required. First, it has to be established if the scanner and camera are steered properly by the software. Previously, the setup had been used in a spiral scan which resulted in good images and an example is shown in figure 21. This means the hardware works. However, this time the scanning will be done in a raster and the software had to be adjusted or replaced. The programming required is quite extensive and errors could exist everywhere. Therefore, the software was first tested by scanning leaves, paper, etc. An intensity image of a raster scan of a leaf is shown in figure 22. While the image is not ideal, it can be clearly seen that this image is distorted somehow. It seems as if the even and uneven horizontal lines are shifted apart. Consequently, a pattern in the image is split into two where the even and uneven horizontal lines each form one pattern. An explanation for this could be in the improper alignment of the pixels. If the first pixels of the image are somehow lost during the scanning or during the creation of the data file, ImageJ will interpret the first pixel in the data file as the first pixel of the image, while it might be the 100th. As a result, all pixels are misplaced. This effect is illustrated schematically in figure 23. The four lines on the top represent the first four horizontal lines of an image. in this figure, a normal image would have its pixel placed in horizontal lines going from 0 to 9. However, when the first two pixels are missing it can be clearly seen what happens to image. Pixels that should be underneath one another are shifted apart. Note that in ImageJ the pixels are placed in the image in a zigzag pattern as seen in section 4. If this weren't the case, a different type of distortion would have taken place if pixels are missing in the beginning of the file. To see if this explanation is sufficient, a new line of programming was written in the ImageJ plugin that would make ImageJ to skip the first pixels of

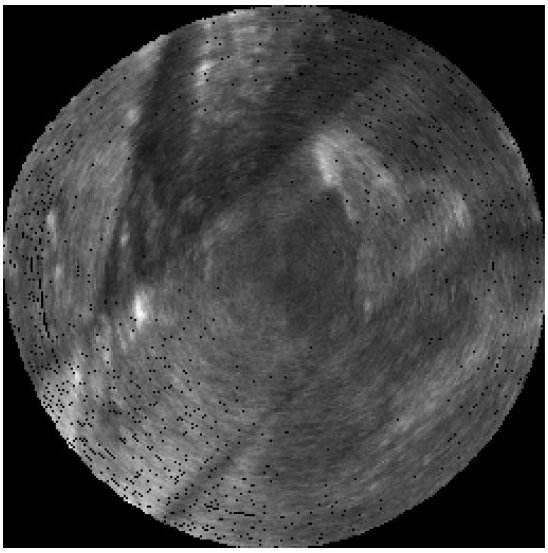

Figure 21: An image as the result of a spiral scan of paper, made 3 July 2012. The detector used in this case was the PMT detector, not the CCT camera. Image taken from Alkemade (2012)[17]

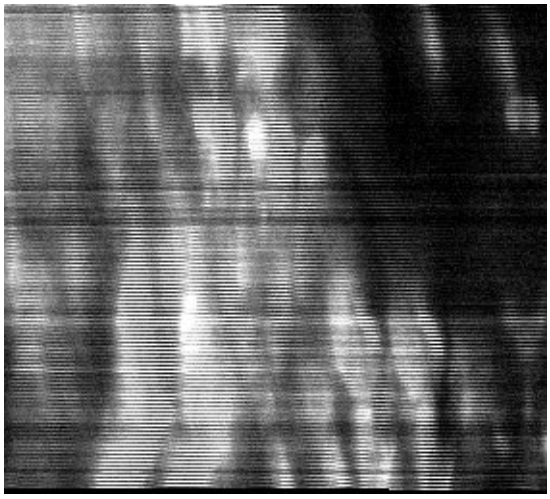

Figure 22: An intensity image as a result of a raster scan of a leaf. Notice the amount of distortion in the image.

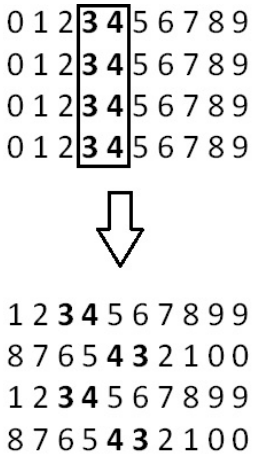


Figure 23: This figure schematically illustrates how missing pixels distort an image. Let the four lines represent the first four horizontal lines of an image, as seen in the top of the figure. The third and fourth pixels of the first line is located directly underneath the third and fourth pixel of the second line. However, when the first two pixels are missing, the lines are shifted as can be seen in the bottom of the figure.

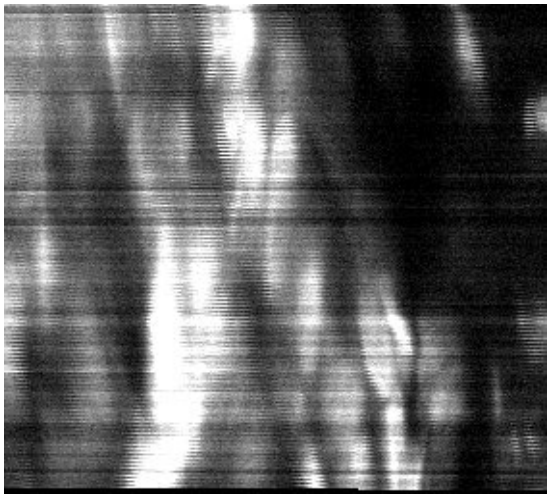

Figure 24: An intensity image of the same data as in fig 22, but this time the first 180 pixel are skipped and the pixel in the top-right corner is, in reality, the 181 pixel. The distortion has only partly disappeared

the data file. If the distortion is indeed (partially) caused by the loss of the first pixels, the distortion should be compromised by skipping pixels so that in total, the entire first horizontal line is deleted. The best result was obtained by omission of the first 180 pixels, as can be seen in figure 24. Apparently, the distortion is partly compensated. However, from this figure it still is not an accurate image and especially at the sides of the image, the patterns are not properly corrected. It was concluded that the distortion had a more complex source. First, a possible delay in the triggering of the camera and the scanner was examined but this wasn't found: both are triggered at the same instant. Next, it was thought the problem was somewhere in the LabView script. Over time, the LabView program had become very complicated and obscure, leaving much room for errors. Furthermore, it could be that the scanning speed of the speed is too high for LabView: after the scan of a pixel, the data of that pixel is send to a buffer where it's temporarily stored, awaiting processing. If the processing is slower than the collection of the data, the buffer might reach its limit and data could be overwritten before its processed. Unfortunately, before the problem could be further researched the setup was moved to the Erasmus Medical Center for the installation of the cover. After the cover was designed, constructed and installed, the power of the laser pulse coming out of the scanner was unexpectedly low. We feared the fiber had been broken and once the scanner was opened, this seemed to be the case. Consequently, no new images could be created after the setup moved to Rotterdam and the project has been significantly delayed. In the end, it is still uncertain if the setup can construct a raster image correctly.

# 6 Further research

Although the setup has not yet produced an accurate image using a raster scan and it has not been tested *in vivo*, these are things that are expected to be accomplished in the future. The new fiber has almost arrived in Rotterdam making the setup will be operational again. By then, the electronics of the setup will be completely revised. The role of LabView is largely reduced and much of its tasks are being replaced by hardware. This will hopefully remove the observed distortion. If this is the case, the experiment with the mice can probably take place in the near future.

# 7 Conclusion

While the project has been delayed extensively, many things have also been achieved in past six months: the ImageJ software has been optimized, the setup has moved to Rotterdam where it has been covered and the construction microscopic plate has started. During this period, I had the opportunity to experience the scientific world and I have learned many different things in the progress. The first thing that comes the mind, is the experience I have gained in writing but I have also received an introduction to programming and I have learned how to work with vulnerable optics and a high power laser. Unfortunately, I have not been able to analyze any data due to delays but even with that in mind, this period has been very fruitful for me as a physics student and I look forward to starting my master next year.

# 8 Acknowledgements

Finally, I would like to thank some people who have made this thesis possible. First I would like to thank Hans Gerritsen, for welcoming me in the Molecular Biophysics department and giving me the chance to learn and work here temporarily. My thanks also go to Gerhard Blab, who I could always ask questions who has introduced me to programming. Then I like to thank Oleg Nadyarnykh for the great time working with him. Finally, it would like to give my deep sincere thanks to Johan van Voskuilen, who was willing to tutor me for the past six months, proofread this thesis multiple times and introduce me to an awesome coffee bar in Rotterdam.

# 9 Appendix

## 9.1 Group velocity dispersion

The dispersion is caused by the fact that photons of different wavelength have a different group velocity in the fiber. The resulting increase of pulse length is usually calculated using the first order dispersion parameter $D$ defined as[22]:

$$D = \frac{\lambda}{c}\frac{\delta^2 n(\lambda)}{\delta\lambda^2} \tag{2}$$

Here, $n(\lambda)$ as is the refractive index of the material as function of the wavelength $\lambda$ and $c$ is the speed of light in vacuum. $D$ stands for the increase in pulse length in femtosecond per nanometer wavelength change per meter fiber length. $n(\lambda)$ is given empirically by Sellmeier equation[24]:

$$n(\lambda) = \sqrt{\sum \frac{\lambda^2 B_i}{\lambda^2 - C_i^2} + 1} \tag{3}$$

In this equation, $B_i$ and $C_i$ are sets of Sellmeier coefficients, which depend on the material in the fiber. After taking the second derivative using Wolfram Mathematica and filling in the correct Sellmeier coefficients of fused silica, one can derive the dispersion in a fiber. Using this method including higher orders, Van Weelden(2010)[23] found a pulse length dispersion of 550 fs per meter silica for a 800 nm laser pulse. Adding the initial pulse length of 140 fs, the length of the laser pulse after passing through the fiber becomes:

$$L = 140 + 550 = 790fs \tag{4}$$

## 9.2 Image of the setup

In figure 25, the setup is shown before it was moved to Rotterdam where the cover was installed. The perspective is similar to the schematic illustration in figure 6 and so are the labels:

1 laser
2 wedge
3 beam expander
4 GVDC
5 spatial mode filter
6 dichroic mirror
7 fiber launcher,fiber & scanner
8 PMT Detector
9 CCT camera

The dichroic mirror is located inside the black cube and the PMT detector is located underneath the blanket. Label 7 points out where the fiber begins and ends. On one end, the objective lens can be seen and on the other end, the scanner located above a temporal microscopic plate.

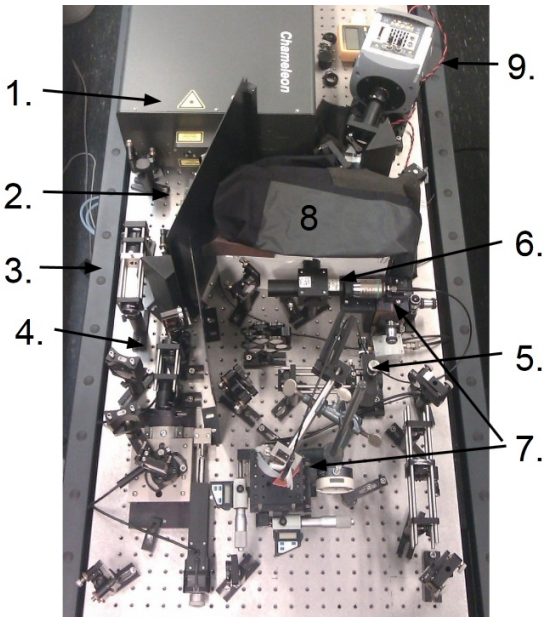


Figure 25: An illustration of the setup before the cover was installed. The perspective is similar to the schematic illustration in figure 6. Alkemade (2012)[17]

# References


[1] P.N. van Kampen & zoon, Amsterdam (1875) *De Gids.* which can be found at `http://www.dbnl.org/tekst/_gid001187501_01/_gid001187501_01_0046.php`

[2] Letter to H. Oldenburg, 9 Oct 1676. *In The Collected Letters of Antoni van Leeuwenhoek* (1957), Vol. **2**, pp. 75

[3] P. Belenky, K.L. Bogan & C. Brenner (2007). "NAD+ metabolism in health and disease". (Trends Biochem. Sci.) vol. **32**, (1):129

[4] J.R. Lakowicz (2006). *Principles of Fluorescence Spectroscopy* (Springer, New York), pp. 1–25.

[5] Image taken from: `http://cleoqels2010.blogspot.nl/2010/05/expo-idea-generation-and-multiphoton.html`

[6] A.K Hadjantonakis & M.E. Dickinson (2003). "Technicolour transgenics: imaging tools for functional genomics in the mouse." (Nat. Rev. Genet.) vol. **4**, pp. 623–625

[7] O. Nadyarnykh & G. Thomas (2012). "Carcinogenic damage to deoxyribonucleic acid is induced by near-infrared laser pulses in multiphoton microscopy via combination of two- and three-photon absorption." (J. Biomed Opt.) vol. **17**, (11)

[8] B.R. Masters & P.T.C. So, eds (2008). *Biomedical Nonlinear Optical Microscopy*, (Oxford University Press, New York) pp. 153–163.

[9] Image taken from: `http://staff.aist.go.jp/narazaki-aiko/SHG_en.html`

[10] Image edited from: `http://chemwiki.ucdavis.edu/Physical_Chemistry/Spectroscopy/Electronic_Spectroscopy/Jablonski_diagram`

[11] Image taken from: `http://www.photobiology.com/v1/sikorski/index.htm`

[12] J.A. Palero (2011). "In vivo monitoring of protein-bound and free NADH during ischemia by nonlinear spectral imaging microscopy." (Biomed Opt express) vol. **2**, (5)

[13] P.A. Jones & Y.A. DeClerck (1980). "Destruction of extracellular matrices containing glycoproteins, elastin and collagen by metastatic human tumor cells."(Cancer Research) vol. **40**, 3222–3227.

[14] Image taken from: `https://www.cvimellesgriot.com/company/Glossary.aspx?Character=K`

[15] image taken from `http://en.wikipedia.org/wiki/File:Laguerre-gaussian.png`

[16] Information taken from a data sheet, supplied by the manufacturer of the fiber. Available at `http://www.nktphotonics.com/files/files/DC-165-16-Passive.pdf` October 16th 2009.

[17] C. Alkemade (2012). "Userfriendly two-photon microendoscope for *in vivo* imaging" Bachelor thesis, Utrecht University.

[18] See 7,12-Dimethylbenz(a)anthracene at Sigma Aldrich `http://www.sigmaaldrich.com/catalog/product/sigma/d3254?lang=en&region=NL`

[19] T.M. Kolb & M.A. Davis (2004) "The Tumor Promoter 12-O-Tetradecanoylphorbol 13-acetate (TPA) Provokes a Prolonged Morphologic Response and ERK Activation in Tsc2-Null Renal Tumor Cells" (Toxicol. Sci.) vol. **81** pp. 233–242

[20] slightly adjusted image taken from the cover of Pink Floyd's ablum: Dark Side Of The Moon (1973)

[21] F. Fereidouni (2012). "Spectral phasor analysis allows rapid and reliable unmixing of fluorescence microscopy spectral images." (Optics Express.) vol. **20**, 12

[22] R. Paschotta (2008). *Encyclopedia of Laser Physics and Technology* (Wiley-VCH, Berlin), article also available at `http://www.rp-photonics.com/group_velocity_dispersion.html`

[23] J. van Weelden (2010). "Instrumentation of a group velocity dispersion compensator." Master thesis, Utrecht University.

[24] W. Sellmeier (1871). "Zur Erklrung der abnormen Farbenfolge im Spectrum einiger Substanzen."( Annalen der Physik und Chemie) vol.**219**, pp. 272–282